Available online at www.sciencedirect.com
SCIENCE DIRECT®
Infrared Physics & Technology 47 (2005) 188–194
INFRARED PHYSICS & TECHNOLOGY
www.elsevier.com/locate/infrared

Terahertz absorption in AlGaAs films and detection using heterojunctions

M.B.M. Rinzan [a], A.G.U. Perera [a,*,1], S.G. Matsik [b], H.C. Liu [c], M. Buchanan [c], G. von Winckel [d], A. Stintz [d], S. Krishna [d]

[a] *Department of Physics and Astronomy, Georgia State University, Atlanta, GA 30303, USA*
[b] *NDP Optronics, LLC., Mableton, GA, 30126, USA*
[c] *Institute for Microstructural Sciences, National Research Council, Ottawa, Canada K1A 0R6*
[d] *Center for High Technology Materials, EECE Dept., University of New Mexico, Albuquerque, NM 87106, USA*

Available online 25 April 2005

Abstract

HEterojunction Interfacial Workfunction Internal Photoemission (HEIWIP) detectors using AlGaAs as both the emitter and the barrier material with different Al fractions for the two layers are demonstrated. The extension of the HEIWIP concept to wavelengths longer than 110 μm in the GaAs/AlGaAs system requires the use of AlGaAs as the emitter material to reduce the barrier height. The p-type doping produces an offset in the valance band between doped and undoped material. The Al fraction difference then gives a valance band offset in the opposite direction, which reduces the total offset. The FIR absorption up to ~400 μm for AlGaAs films with different Al fractions and doping are presented. The absorption in the films with low Al fraction (1%) shows little variation from comparable GaAs films while for 20% Al, the absorption is reduced. The spectral results on a device with 12% Al emitters and 11% Al barriers have shown a response of 0.6 A/W at 30 μm with $D^* = 3 \times 10^{10}$ Jones measured at 5 K. The low responsivity is due to the reduced number (3) of emitters in the test device, and when scaled for the number of emitters this is comparable to results obtained from GaAs/AlGaAs HEIWIP detectors. Based on these results, a design for a 300 μm detector is presented and potential difficulties in growth and fabrication such as dopant migration are discussed.

PACS: 85.60.Gz; 78.66.Fd; 78.67.Pt

Keywords: Terahertz detectors; AlGaAs; Heterojunction; Absorption; Refractive index

* Corresponding author. Tel.: +1 404 651 2279; fax: +1 404 651 1427.
E-mail address: uperera@gsu.edu (A.G.U. Perera).
[1] Also at NDP Optronics LLC.

1350-4495/$ - see front matter © 2005 Elsevier B.V. All rights reserved.
doi:10.1016/j.infrared.2005.02.025

1. Introduction

Far InfraRed (FIR) or Terahertz (THz) detectors [1–6] have attracted increased attention for use in both astronomy and other applications. The astronomical interest stems from the many different objects which radiate in the far infrared: dust disks [7,8] and gas molecules such as CO and HD [9] being important examples. THz detectors will be important in studies of planet formation around nearby stars, and the outer planets and their moons. Also, there is a potential for use in early universe studies as the near and mid-infrared emissions of high red shift objects can end up in the THz.

In this paper, results are presented on a novel approach to the development of FIR/THz detectors based on using AlGaAs both as emitters and as barriers. The proposed design is a modification of the standard heterojunction interfacial workfunctions internal photoemission (HEIWIP) detectors [10]. In the standard HEIWIP detectors, doped GaAs emitter layers alternate with undoped $Al_xGa_{1-x}As$ barrier layers. The detection mechanism involves free-carrier absorption in the emitters, internal photoemission across the emitter/barrier interface and collection of the emitted carriers at the contacts. The threshold wavelength λ_0 is determined from the workfunction Δ by λ_0 (μm) = 1240/Δ (meV), where $\Delta = \Delta_x + \Delta_d + \Delta_b$, with Δ_x the contribution from the Al fraction, Δ_d the contribution from the doping, and Δ_b the contribution from the band bending in the barrier as shown in Fig. 1(a). In the standard HEIWIP design, $\Delta_b < 1$ meV (for 1×10^{15} cm^{-3} residual doping) and can be ignored, $\Delta_d \sim 9$–10 meV [11] (for $1-8 \times 10^{18}$ cm^{-3}), and $\Delta_x = 530x$ meV based on 35% offset in the valence band. As x is decreased λ_0 increases, however due to Δ_d there is a limit of $\lambda_0 \sim 110$ μm associated with the MBE growth limit for the lowest Al fraction ($x = 0.005$). At $x = 0$ a homojunction detector [12] will be realized. Although increasing the doping would reduce Δ_d, for homojunctions, the transitions between light and heavy holes will still limit λ_0 to 70–100 μm [13]. An alternate approach explored here is to use $Al_xGa_{1-x}As$ in both the emitters and the barriers as shown in Fig. 1(b). If x is larger in the emitter than in the barrier, $\Delta x < 0$, giving $\Delta_x = \Delta x \times 530$ meV < 0 and $\Delta < \Delta_d$, avoiding the limits for GaAs emitters.

2. Doped AlGaAs absorption

As a first step towards developing a HEIWIP detector using AlGaAs emitters, the absorption was studied in doped AlGaAs thin films. Four p-type $Al_xGa_{1-x}As$ thin films were grown by MBE on 520-μm-thick semi-insulating GaAs

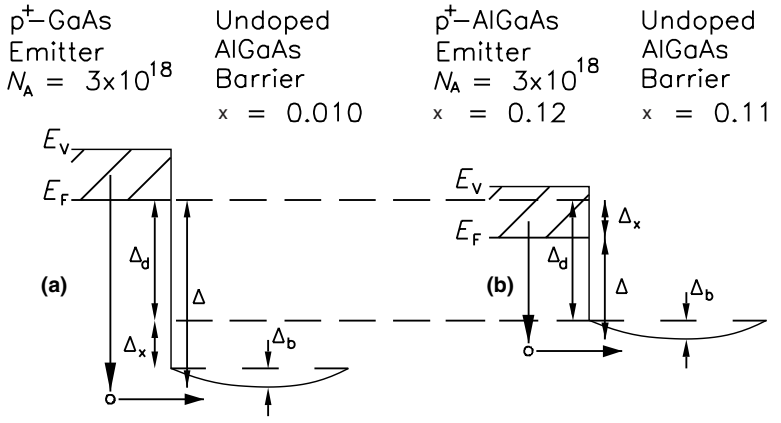

Fig. 1. (a) The band diagram for the standard HEIWIP design showing the contributions to Δ from doping (Δ_d), Al fraction (Δ_x) and the band bending due to residual doping (Δ_b). In the standard approach $\Delta > \Delta_d + \Delta_b$. (b) The modified design with AlGaAs emitter and barriers. Here, $\Delta_x < 0$ so Δ can be reduced to obtain $f_0 < 2.7$ THz ($\lambda_0 > 110$ μm).

Table 1
Parameters of the thin film samples measured

Sample	x	p ($\times 10^{18}$ cm^{-3})	f_p (THz)	λ_p (μm)
1442	0.01	3	6.6	45.2
1443	0.01	5	8.6	35.0
1444	0.01	8	10.9	27.6
1446	0.20	5	8.3	36.3

The 1-μm thick Be doped $Al_xGa_{1-x}As$ films were grown on 520-μm-thick semi-insulating GaAs substrate. Here, x is the Al fraction, p is the acceptor doping density, and f_p and λ_p are the plasma frequency and the wavelength of the free holes, respectively.

wafers with the relevant parameters shown in Table 1. Room temperature reflection and transmission measurements were made for three films with 3, 5, and 8×10^{18} cm^{-3} doping densities and 0.01 Al fraction, and for two films with Al fractions 0.01 and 0.20 with 5×10^{18} cm^{-3} doping density. Experimental IR absorption of the film layers were obtained from the transmission and reflection data.

Fig. 2(a) shows the fraction of the incident IR radiation absorbed in $Al_{0.01}Ga_{0.99}As$ films for three different doping concentrations. For a fixed doping density, the absorption approaches a constant value, ~20–25%, in the region 1.5–0.75 THz (200–400 μm). The ripples towards the FIR end are due to the Fabry-Pérot interference from the 520 μm-thick substrate. Although the absorption is expected to increase with increased doping, measurements showed the reflection also increases with doping in the range 3–0.75 THz (100–400 μm). The increased reflection offsets most of the absorption gains giving only a small increase in the absorbed fraction. Reflection losses could be reduced by employing methods such as antireflection coatings for the desired wavelength ranges. These results for $Al_xGa_{1-x}As$ with $x = 0.01$ are similar to those for doped GaAs [11]. As the Al fraction is increased the absorption will decrease, with a 10–20% decrease in absorption at $x = 0.20$ as shown in Fig. 2(b).

The refractive index was calculated using material parameters determined from fitting the reflectance spectra. Beyond 100 μm a significant change with the doping in the layer occurred as shown in Fig. 3(a). However, as can be seen in Fig. 3(b), there is no significant change in the index with varying Al fraction. This indicates that varying the overall Al fraction while maintaining the difference between the layers will not have a significant effect on the detector performance due to the refractive index.

3. Device design

The detector structure (HE0403) shown in Fig. 4 consisted of, from top to bottom, a 1×10^{19} cm^{-3} Be-doped 1000 Å GaAs top contact,

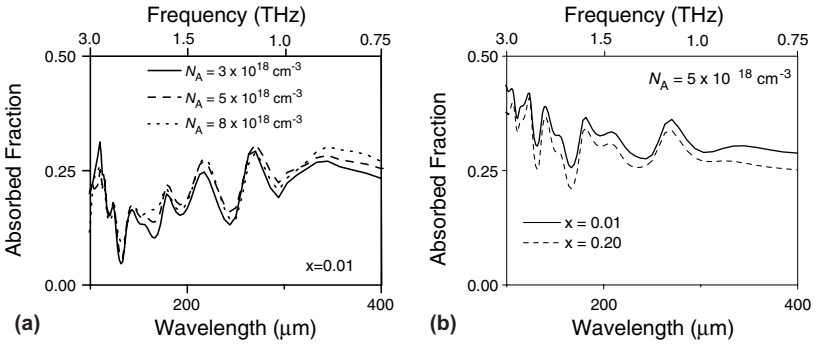

Fig. 2. (a) Fraction of incident light absorbed measured at room temperature for three p-doped (3, 5, and 8×10^{18} cm^{-3}) $Al_{0.01}Ga_{0.99}As$ thin films in the range 60–0.75 THz (5–400 μm). The sharp drop is due to the strong photon–optical phonon interaction reducing the transmission below the noise level of the FTIR. While the absorption coefficient increases with the concentration, the increase in the region 3–0.75 THz (100–400 μm). While the absorption coefficient increases with the concentration, the increase of the absorbed fraction in the region 3–0.75 THz (100–400 μm) is offset by the reflection loss. (b) Fraction of incident light absorbed measured at room temperature for p-doped 5×10^{18} $Al_xGa_{1-x}As$ films with $x = 0.01$ and 0.20. The increased Al fraction has decreased the absorption by 10–20%.

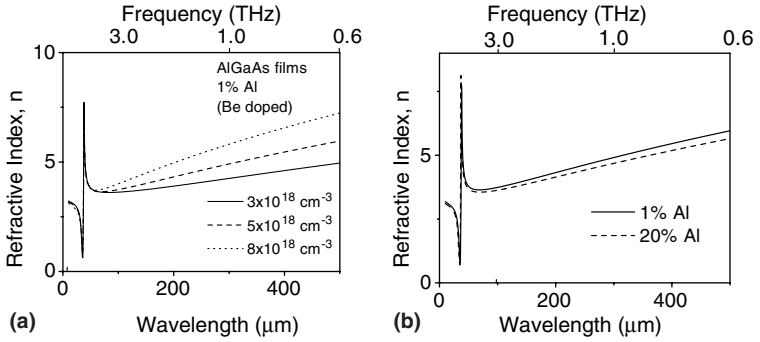

Fig. 3. (a) The variation of calculated refractive index with doping over the frequency/wavelength range of interest. For 1% Al, the index does not vary significantly at shorter wavelengths but does at longer wavelengths. (b) The effects of increasing the Al fraction from 1% to 20%. This produces only a small change in the index.

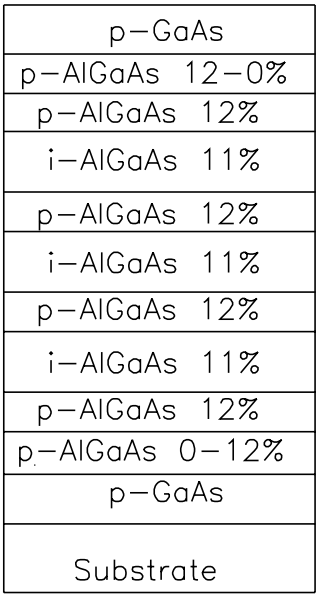

Fig. 4. The structure for the detector sample HE0403 using AlGaAs both as emitters and as barriers. The difference in Al fraction between the layers contribute to the workfunction.

a 1×10^{19} cm^{-3} Be-doped 200 Å $Al_xGa_{1-x}As$ layer graded from $x = 0.00$ to 0.12, a 1×10^{19} cm^{-3} Be-doped 300 Å $Al_{0.12}Ga_{0.88}As$ layer to serve as the top emitter, 3 periods of 2000 Å $Al_{0.11}Ga_{0.89}As$ barriers and 3×10^{18} cm^{-3} Be-doped 300 Å $Al_{0.12}$-$Ga_{0.88}As$ emitters, a 1×10^{19} cm^{-3} Be-doped 200 Å $Al_xGa_{1-x}As$ layer graded from $x = 0.12$ to 0.00, and a 1×10^{19} cm^{-3} Be-doped 7000 Å GaAs bottom contact. The graded layers served as a transition between the high Al fraction of the detector and the GaAs contacts which were selected to avoid any difficulties with deterioration of AlGaAs when exposed to atmosphere. The spectral response was measured with a FTIR spectrometer using a Si bolometer as the reference detector. The experimental spectral response of the device is shown in Fig. 5. The peak response was 0.6 A/W at 10 THz (30 μm) with NEP of 2×10^{-12} W/Hz$^{1/2}$ giving $D^* = 3\times10^{10}$ Jones measured at 5 K.

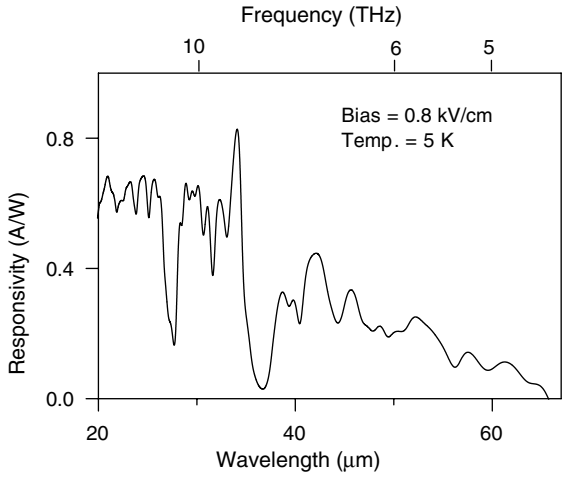

Fig. 5. Response curves for the sample HE0403 showing a peak response of 0.6 A/W at 10 THz (30 μm) and 5 K with NEP = 2×10^{-12} W/Hz$^{1/2}$ and $D^* = 3\times10^{10}$ Jones. The threshold indicated by the vertical arrow is 4.6 THz (65 μm). The sharp drops at 8 and 11 THz (36 and 27 μm) is due to the AlAs like phonon in the AlGaAs emitters.

The low responsivity is due to the small number (3) of emitters in the detector. When the responsivity is scaled up to account for the number of layers it is comparable to the results obtained from previous detectors with a threshold wavelength of 65 μm [14].

4. Band bending in HEIWIP structures

The expected Δ between the 12% Al doped emitters and the 11% undoped barriers is 4.8 meV. However, the observed threshold of 4.6 THz corresponds to a Δ of 17 meV. One possible explanation could be the band bending due to residual doping in the barriers, which can increase Δ, increasing the threshold frequency. The bending is produced by unintentional doping in the barrier region which can be due to compensating ionized doping in the barriers. The bending from the residual doping will be small unless thick barrier regions are used. For the thicker (2000 Å) barriers in the present sample, $\Delta_b = 10$–15 meV is expected at zero bias. This band bending can be reduced to 3–5 meV by applying a bias field. However, the field required for a reduction of Δ_b to zero gives a large dark current, and hence is not practical.

The spectral results from sample HE0403 agrees with a significant band bending effect, where Δ is increased by ~15 meV. The threshold had only a small variation with bias (not shown) indicating that dopant migration was an important factor in this case. SIMS data for sample HE0403 with two key features as shown in Fig. 6 verifies this explanation. First the diffusion of Be past the emitter/barrier interface will lead to enhanced band bending. This means that this sample is behaving as if it is a homojunction rather than a heterojunction. Second is the nonuniform Al fraction in the barrier layers. This will cause additional variation in the barrier shape and due to the asymmetric Al fraction in the barrier, an asymmetric barrier shape is produced.

5. Increased operating temperature

The asymmetric band shape can be used to increase the operating temperatures of the detectors. This asymmetry introduces a small photovoltaic component to the response which leads to higher temperature operation than is observed for purely photoconductive detectors. A comparison of the $Al_xGa_{1-x}As$ emitter detector (HE0403) with a second similar threshold detector using GaAs emitters (2409) [14], for which diffusion was not a significant problem, can be used to demonstrate this advantage.

Plots of dark and photocurrent at different temperatures for samples HE0403 and 2409 are shown in Fig. 7. The BLIP temperature (estimated from the temperature at which the dark and photocurrents are equal) is 15 ± 1 K for 2409 and 22 ± 1 K for HE0403. The increase in the BLIP temperature of HE0403 is due to drift effects of carriers that are excited to just above the barrier. It is easier for the carriers to move in one direction than in the other direction, due to the

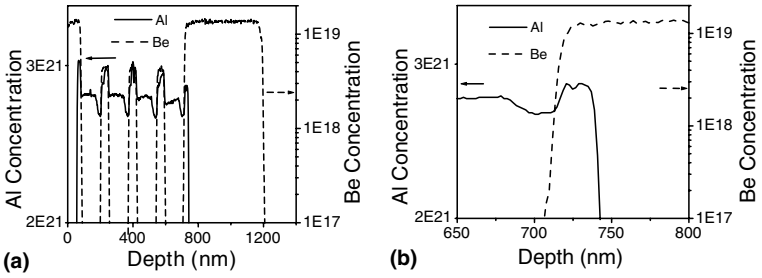

Fig. 6. (a) SIMS data for Al and Be concentration in the sample HE0403 showing enhanced diffusion of Be. Also visible is the variation in Al in the barrier region that enhances the barrier asymmetry. Note that due to the band edge shift from the doping, the lower Al region corresponds to the barrier. (b) An enlarged view of the interface at the bottom contact showing the larger diffusion of the Be.

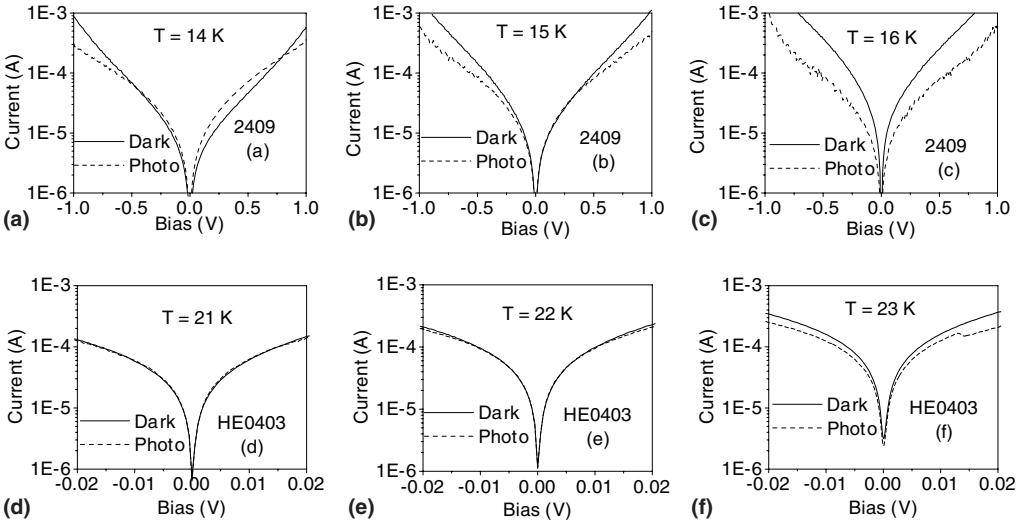

Fig. 7. Plots of dark and 300 K background photocurrent for sample 2409 at (a) 14, (b) 15, and (c) 16 K, and sample HE0403 at (d) 21, (e) 22, and (f) 23 K. The BLIP temperature based on the photocurrent matching the dark current is 15 K for 2409 and 22 K for HE0403. The threshold frequencies are the same and the increase for sample HE0403 is believed to be due to the asymmetric barriers resulting from dopant diffusion and the Al fraction variation.

asymmetry in the barrier. After carriers enter the barrier region, they will slowly relax and loose energy. Only if the carrier energy is above the barrier at its maximum location, will the carrier continue on through the barrier. If the energy is lower, they will be reflected back to the previous emitter region. For a symmetric barrier, the carriers moving in both direction will relax by the same amount so that the contributions to the current will be equal. However, for an asymmetric barrier, more of the carriers that have to travel farther will relax to a lower energy so that they will be reflected as shown

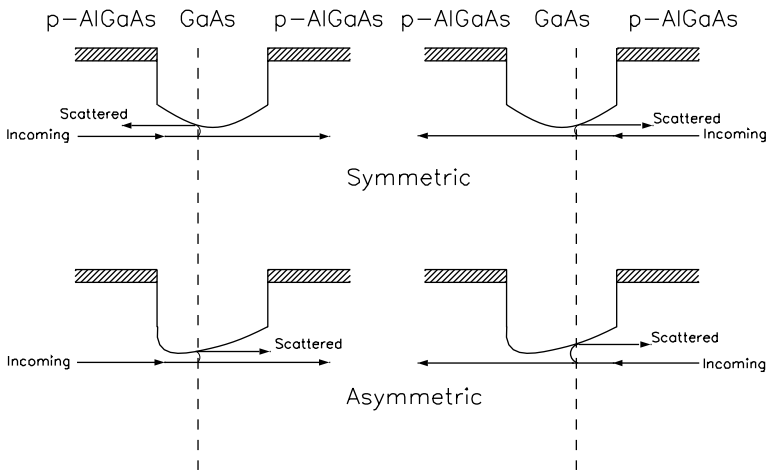

Fig. 8. Band diagram for a symmetric and asymmetric barrier showing the effect of the asymmetry on carriers passing over the barrier. The curved sections of the carrier path represent a scattering event at the same distance from the interface. For the symmetric barrier, the carriers injected from both directions will be reflected back to the emitter after scattering. For the asymmetric barrier, the scattered carriers from the side farthest from the maximum are reflected, while the scattered carriers from the other side pass through. The vertical dashed lines indicate where the scattering is assumed to occur. These locations are the same distance from the interface.

in Fig. 8. As a result, the carriers injected from the left in the figure pass through and are collected at the far contact while the carriers injected in the opposite direction are stopped and return to the original contact. The resulting current causes a small photovoltaic response in the detector. The photovoltaic response increases the BLIP temperature of the detector. At high temperatures, the effect of the slant is neutralized by the large number of high energy carriers so that, eventually, the photovoltaic response becomes negligible.

6. Conclusions

Results have been presented showing FIR absorption in AlGaAs films. Although the absorption is reduced compared to GaAs, it remains large enough to be used in a detector. In particular, doped AlGaAs will prove useful in extending the frequency range beyond 2.7 THz (110 μm). A detector with a responsivity of 0.6 A/W and a threshold frequency of 4.6 THz (65 μm) using AlGaAs in the emitters and barriers has been demonstrated. The threshold was limited by dopant migration, but devices adjusted for the migration should lead to $f_0 < 2.7$ THz ($\lambda_0 > 110$ μm). Asymmetries in the barriers provided increased operating temperatures, giving a BLIP temperature of 22 K compared to 15 K for similar devices.

Acknowledgements

This work was supported in part by the NSF under grant #ECS-0140434, NASA under SBIR contract NNC04CA95C, and DOE/BES under grant DE-FG03-02ER46014.

References

[1] H.C. Liu, C.Y. Song, A.J. Spring Thorpe, J.C. Cao, Appl. Phys. Lett. 84 (2004) 4068.
[2] X.W. Mi, J.C. Cao, C. Zhang, J. Appl. Phys. 95 (2004) 1191.
[3] C. Cates, J.B. Williams, M.S. Sherwin, K.D. Maranowski, A.C. Gossard, SPIE 3617 (1999) 58.
[4] N.E.I. Etteh, P. Harrison, IEEE J. Quantum Electron. 37 (2001) 672.
[5] S.G. Matsik, M.B.M. Rinzan, D.G. Esaev, A.G.U. Perera, H.C. Liu, M. Buchanan, Appl. Phys. Lett. 84 (2004) 3435.
[6] S. Krishna, G. von Winckel, S. Raghavan, A. Stintz, G. Ariyawansa, S.G. Matsik, A.G.U. Perera, Appl. Phys. Lett. 83 (2003) 2745.
[7] P. Garcia-Lario et al., Astrophys. J. 513 (1999) 941.
[8] H. Izumuira et al., Astron. Astrophys. 315 (1996) L221.
[9] B. Bezard, D. Gautier, A. Marten, Astron. Astrophys. 161 (1986) 387.
[10] A.G.U. Perera, S.G. Matsik, B. Yaldiz, H.C. Liu, A. Shen, M. Gao, Z.R. Wasilewski, M. Buchanan, Appl. Phys. Lett. 78 (2001) 2241.
[11] A.G.U. Perera, Semiconductor photoemissive structures for far infrared detection, in: A.G.U. Perera, H.C. Liu, M.H. Francombe (Eds.), Handbook of Thin Film Devices: Semiconductor Optical and Electro Optical Devices, Academic Press, 2001.
[12] A.G.U. Perera, H.X. Yuan, M.H. Francombe, J. Appl. Phys. 77 (1995) 915.
[13] A.G.U. Perera, S.G. Matsik, M.B.M. Rinzan, A. Weerasekara, M. Alevli, H.C. Liu, M. Buchanan, B. Zvonkov, V. Gavrilenko, Infrared Phys. Technol. 44 (2003) 347.
[14] S.G. Matsik, M.B.M. Rinzan, A.G.U. Perera, H.C. Liu, Z.R. Wasilewski, M. Buchanan, Appl. Phys. Lett. 82 (2003) 139.